Science Advances

AAAS

advances.sciencemag.org/cgi/content/full/3/3/e1602811/DC1

Supplementary Materials for

Atomically engineered electron spin lifetimes of 30 s in silicon

Thomas F. Watson, Bent Weber, Yu-Ling Hsueh, Lloyd L. C. Hollenberg,
Rajib Rahman, Michelle Y. Simmons

Published 31 March 2017, *Sci. Adv.* **3**, e1602811 (2017)
DOI: 10.1126/sciadv.1602811

This PDF file includes:

Supplementary Materials

section S1. Extraction of the electron temperature, gate lever arms, and addition energies of D1 and D2

The electron temperature T_e can be extracted from the thermal broadening of the Fermi level of the SET island [*24*]. Figure S1a shows a close up of a break in a SET transport line due to the 1st electron transition on D1. Along the SET line in the direction of the blue arrow in fig. S1a the position of the electrochemical potential of D1 is lowered from above to below the electrochemical potential of the SET which remains fixed as shown in fig. S1b. Figure S1c shows the normalised time averaged current measured along the blue arrow for a mixing chamber temperature of T_M = 100 mK. The normalised current is plotted as a function of the change in voltage δV_1 on G1 from the point in gate space where the electrochemical potential of D1 and the SET are aligned (red circle in fig. S1a). The normalised current reflects the occupation probability of the SET which can be fit with a Fermi distribution

$$I = \frac{1}{e^{(\alpha_{D1}\delta VG1)/k_bT_e} + 1} \qquad (1)$$

where k_b is the Boltzmann constant and α_{D1} is the gate lever arm to D1 used to convert a change in voltage on G1 in the direction of an SET transport line to an energy. From this fit we extract the constant $a = \alpha_{D1}/k_bT_e$. In fig. S1d we plot T_e/α_{D1} as a function of the mixing chamber temperature. At $T_M \geq 100$ mK, T_e/α_{D1} increases linearly as the bath temperature is equal to the electron temperature, $T_e = T_M$. From the inverse of the slope m of the linear fit to the data for $T_M \geq 100$ mK we can extract the lever arm $\alpha_{D1} = 1/m = 0.064 \pm 0.002$. We repeat these measurements for the 1st electron transition of D2. From the plot of T_e/α_{D2} vs T_M shown in fig. S1e we extract the lever arm of the G1 to D2 in the direction of a SET transport line to be $\alpha_{D2} = 1/m = 0.079 \pm 0.002$. For both measurements, at $T_M \leq 100$ mK, T_e/α deviates from the linear behaviour as the electron temperature no longer decreases by the same amount as the bath temperature. From the saturation value of T_e/α for D1 and D2 we estimate the electron temperature to be $T_e \approx 100$ mK.

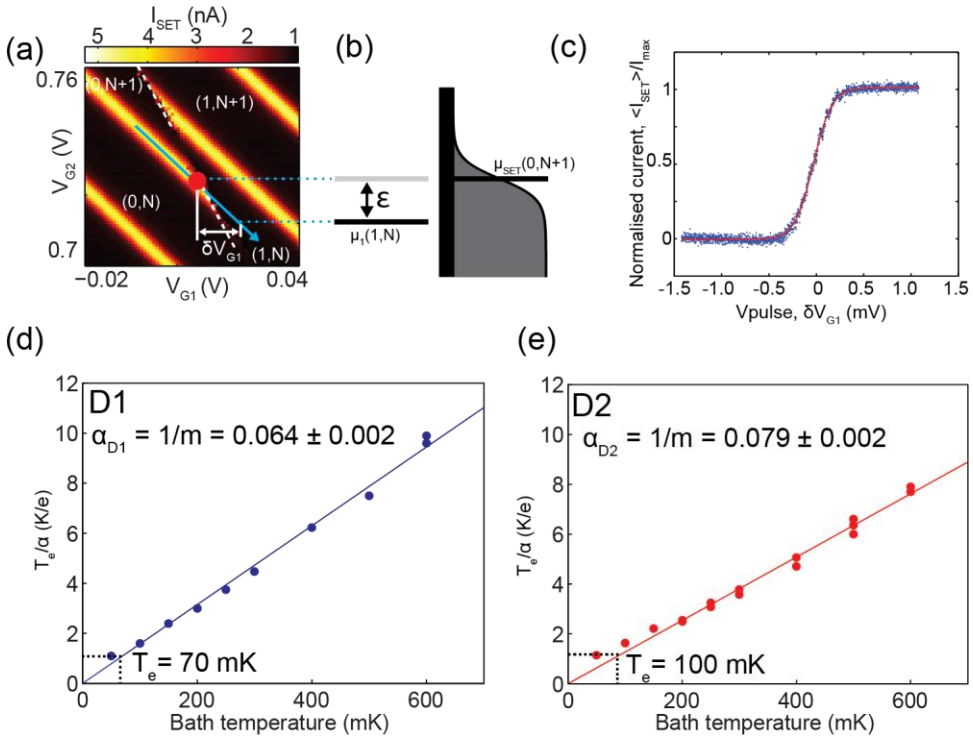

fig. S1. Extraction of the electron temperature and gate lever arms from the thermal broadening of the SET Fermi level. (**a**) Close up of a break in an SET transport line due to the 0 to 1 electron transition on D1. The occupation number on D1 and the SET is indicated in brackets. (**b**) Along the blue line the electrochemical potential of D1 is lowered from above to below that of the SET electrochemical potential which remains fixed. At the red circle the electrochemical potential of D1 and the SET are aligned. (**c**) The normalised time averaged current $\langle I_{SET}\rangle/I_{max}$ along the blue line in (a) for a mixing chamber temperature of T_M = 100 mK. The current corresponds to the occupation probability of the SET which follows a Fermi distribution. (**d**, **e**) Fitting the distribution with a Fermi function we extract the parameter T_e/α which we plot as a function of the mixing chamber temperature for (d) D1 and (e) D2. From these plots we extract the electron temperature and gate lever arms.

The addition energies of D1(2) are extracted from the transport stability diagram in fig. S2a by measuring the change in voltage ΔV_{add} ($n - 1 \leftrightarrow n$) along an SET line between successive charge transitions of D1(2). The addition voltages, ΔV_{add} ($1 \leftrightarrow 2$) and ΔV_{add} ($2 \leftrightarrow 3$) to add the second and third electron on D2 is indicated in fig. S2a, d by the black arrows. The addition voltages of D1(2) are converted to addition energies by multiplying by the lever arm $\alpha_{D1(2)}$ calculated from the temperature dependence in fig. S1. The extracted lever arms, addition voltages, and the addition energy spectrum of both donor dots, D1 and D2, are summarised in table S1 for two different device cool downs. In the second cool down the lever arm was measured at each electron transition and found to be relatively constant.

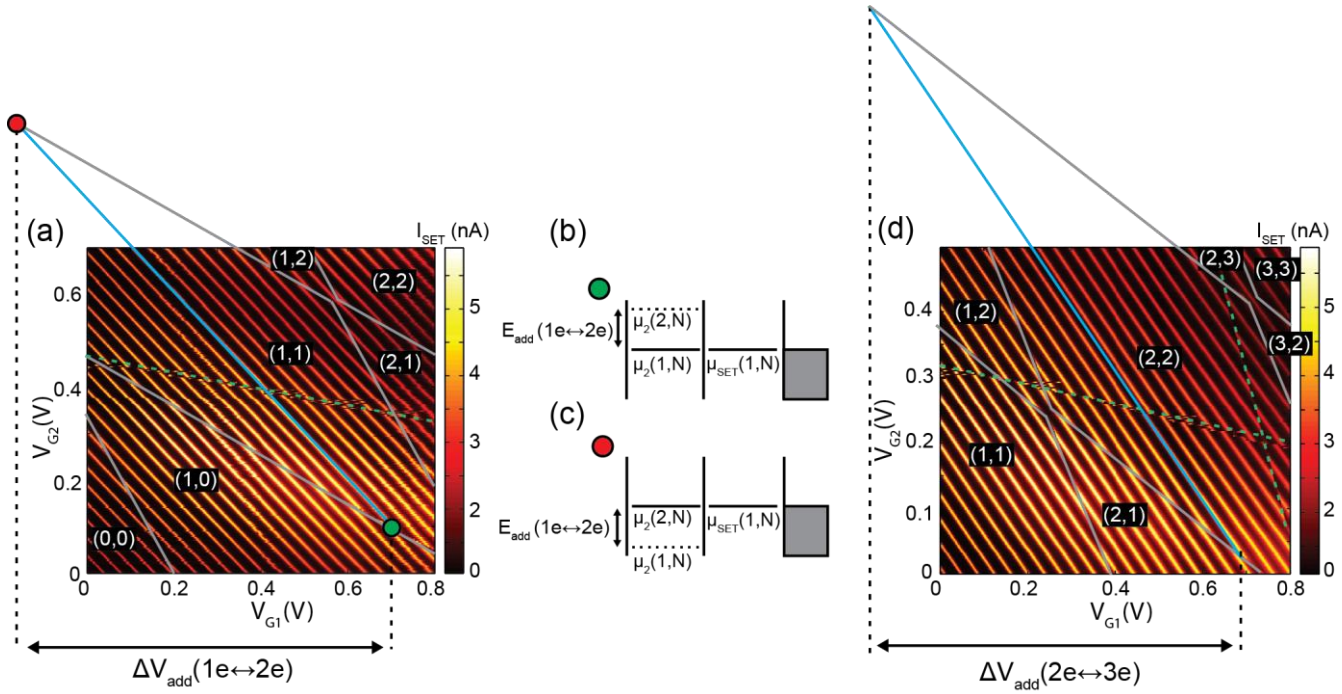

fig. S2. Extraction of the addition energy for the second and third electrons on D2. (**a**) Stability map taken at V_T = 0 mV showing the first and second electron transition of D2. The addition energy of the second electron on D2 is extracted from the change in voltage ΔV_{add} (1e ↔ 2e) from the green to the red circle. Energy level diagrams show that moving from the (**b**) green circle to the (**c**) red circle results in a shift in the D2 electrochemical potential by the addition energy E_{add} (1e ↔ 2e). (**d**) Stability map taken at V_T = 400 mV showing the extraction of the addition energy of the third electron on D2. Two additional transitions indicated by the green dotted lines are observed that have a different charge transfer signals and slopes compared to D1 and D2 and are due to traps near the SET.

The exact donor numbers of D1 and D2 are estimated by comparing the experiment addition energies with those calculated with atomistic tight-binding modelling with the NEMO-3D code [*15*]. In the model, 2P, 3P, and 4P donor atoms were distributed at substitutional lattice sites within the lithographically defined quantum dot with 1 nm added in all directions to take into account donor diffusion. The donors were embedded within a 30 × 30 × 30 nm^3 simulation domain represented by a screened and truncated Coulomb potential at a substitutional lattice site which was parametrised to give the experimental ground-state energy of 45.6 meV [*32*] for a single donor in bulk [*33*]. The binding energies for different donor numbers and configurations were calculated via a self-consistent Schrödinger-Poisson solver with electron-electron interactions included through a local density approximation (LDA) Ansatz [*34*]. Figure S3a–c shows the modelled addition energies (grey bands) for a 2P, 3P and 4P donor dot compared to the experimental addition energies extracted for D1 (red squares) and D2 (blue squares). The shaded grey bands represent the percentile likelihood (%) of addition energies based on all possible donor configurations within 1 nm of the lithographic patch. The addition energies of D1 and D2 match most closely with those calculated for a 3P and 2P donor dot, respectively.

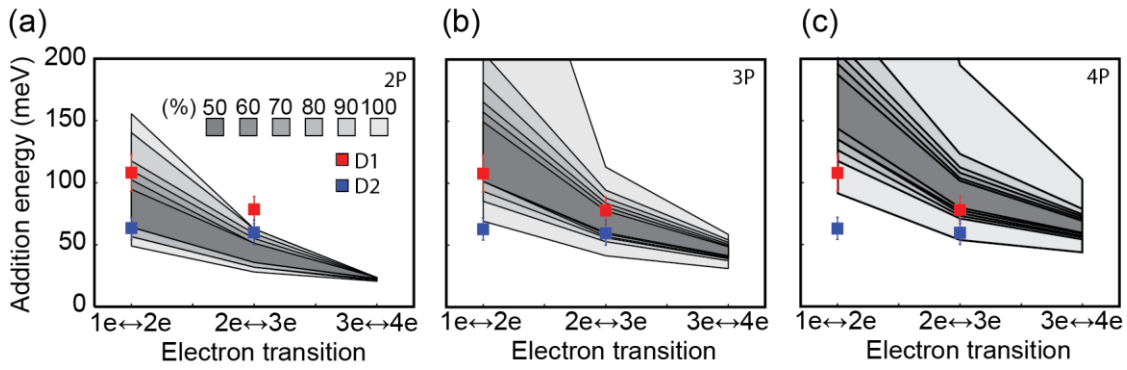

fig. S3. Atomistic tight-binding calculations of the addition spectrum of 2P, 3P, and 4P donor dots. (**a**–**c**) The percentile likelihood (%) (shaded grey bands) of the addition energy as a function of electron number are shown for a (a) 2P, (b) 3P, and (c) 4P donor dot. Comparing the addition energies of D1 (red square) and D2 (blue square) with the modelled addition energies we determine D1 and D2 are most likely 3P and 2P donor dots, respectively.

table S1. Comparison of lever arms (α), addition voltages (ΔV_{add}), and addition energies (E_{add}) of D1 and D2 for each electron transition for two different cooldowns.

Electron transition	α	ΔV_{add} (V)	E_{add} (meV)	$E_{add,\ ave}$ (meV)
D1, 1e ↔ 2e	0.064 ± 0.006 0.063 ± 0.003	1.69 ± 0.08 1.72 ± 0.09	108 ± 15 108 ± 11	108 ± 15
D1, 2e ↔ 3e	0.064 ± 0.006 0.061 ± 0.003	1.22 ± 0.06 1.35 ± 0.07	78 ± 11 82 ± 8	78 ± 12
D2, 1e ↔ 2e	0.071 ± 0.004 0.080 ± 0.003	0.84 ± 0.04 0.82 ± 0.04	60 ± 6 66 ± 6	63 ± 9
D2, 2e ↔ 3e	0.071 ± 0.004 0.079 ± 0.003	0.79 ± 0.04 0.84 ± 0.04	56 ± 6 66 ± 6	61 ± 11

section S2. Fidelity of the sequential readout of D1 and D2

In this section we assess the measurement fidelity of the readout of the 1st electron bound to D1 and D2. The measurement fidelity is the probability that the assignment of a $|\uparrow\rangle$ or $|\downarrow\rangle$ electron state from the SET current response during readout is correct. The signature of a $|\uparrow\rangle$ electron is a single current pulse during the readout time Δt which is due to the $|\uparrow\rangle$ electron tunnelling out of the donor turning the SET current on and a $|\downarrow\rangle$ electron tunnelling back onto the donor turning the SET current off. To calculate the fidelity we analyse 7500 current traces where we perform the sequential readout of D1 followed by D2. Figure S4a shows 250 of these current traces. In these measurements a constant magnetic field of B = 1.5 T was applied as this is typically used during electron spin resonance (ESR) of an electron spin qubit [*1*].

The spin dependent tunnel times of the $|\uparrow\rangle$ and $|\downarrow\rangle$ electron in and out of the donor during spin readout are necessary to determine the fidelity of the readout. Figure S4b shows the real-time SET current during the readout of a $|\uparrow\rangle$ electron. The start and duration of the single current pulse are determined by the $|\uparrow\rangle$ tunnel out time $\tau_{\uparrow,out}$ and $|\downarrow\rangle$ tunnel in time $\tau_{\downarrow,in}$, respectively (fig. S4c). Figure S4e, f show

histograms of the tunnel times $\tau_{\uparrow,out}$ and $\tau_{\downarrow,in}$ during readout of D1 and D2. From exponential fits of these histograms we extract the characteristic tunnel times to be $\tau_{\uparrow,out} = 5.7 \pm 0.4$ ms, $\tau_{\downarrow,in} = 11.6 \pm 1.0$ ms for D1 and $\tau_{\uparrow,out} = 5.9 \pm 0.4$ ms, $\tau_{\downarrow,in} = 8.2 \pm 0.8$ ms for D2.

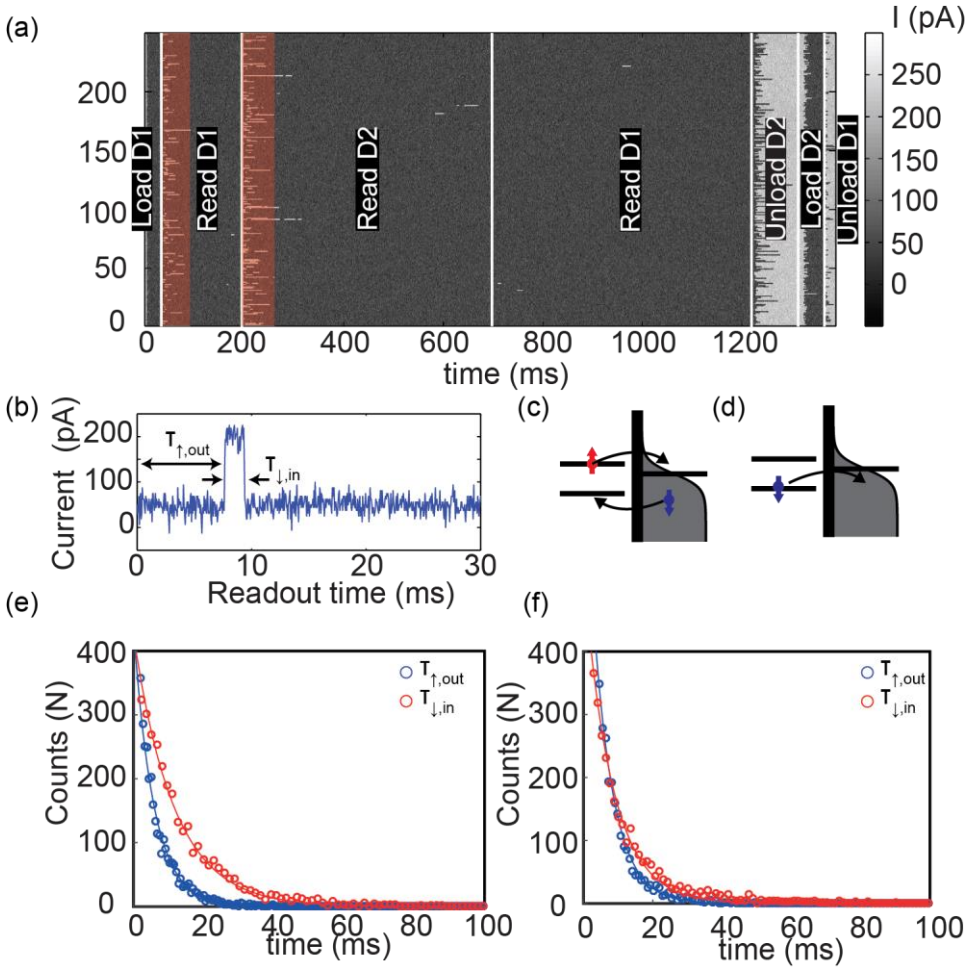

fig. S4. Extraction of the spin-dependent tunnel times during readout of D1 and D2. Map showing 250 current traces during the sequential readout of D1 and D2. These traces are part of a larger data set of 7500 readout cycles used for the extraction of the spin dependent tunnel times and fidelity analysis of the readout of D1 and D2. The red shaded panels show the readout time Δt which was optimised post-processing to maximise the fidelity. (**b**) The start and duration of the single current pulses are determined by the $|\uparrow\rangle$ tunnel out time $\tau_{\uparrow,out}$ and the $|\downarrow\rangle$ tunnel in time $\tau_{\downarrow,in}$, respectively. (**c**) Energy level diagram showing the electrochemical potential of the donor and the SET during readout. (**d**) Due to the thermal broadening of the SET there is a finite probability that a $|\downarrow\rangle$ electron tunnels out of the donor to the SET during readout. (**e**–**f**) Histograms of the tunnel times $\tau_{\uparrow,out}$ and $\tau_{\downarrow,in}$ during the readout of (e) D1 and (f) D2. From exponential fits of these histograms (solid lines) we extract the characteristic spin dependent tunnel times to be $\tau_{\uparrow,out} = 5.7 \pm 0.4$ ms, $\tau_{\downarrow,in} = 11.6 \pm 1.0$ ms for D1 and $\tau_{\uparrow,out} = 5.9 \pm 0.4$ ms, $\tau_{\downarrow,in} = 8.2 \pm 0.8$ ms for D2.

In fig. S4a the current traces that do not have a current pulse that starts during the readout time Δt correspond to a $|\downarrow\rangle$ electron. There is a finite probability that a $|\downarrow\rangle$ electron tunnels out of the donor dot due to the thermal broadening of the SET (fig. S4d). The $|\downarrow\rangle$ tunnel out time for D1 and D2 are

extracted from the data in fig S4a using two slightly different methods. For D2, we estimate $\tau_{\downarrow,out}$ by counting tunnelling events after a time t_1 where all the $|\uparrow\rangle$ electrons have tunnelled from the donor, $t_1 >> \tau_{\uparrow,out}$. During the readout of D1, 12 out of the 3250 $|\downarrow\rangle$ electrons tunnel out of the donor between the times t_1 = 100 ms and t_2 = 500 ms. Therefore the tunnel out time $\tau_{\downarrow,out}$ is found by solving

$$\exp(\frac{-t_1}{\tau_{\downarrow,out}}) - \exp(\frac{-t_2}{\tau_{\downarrow,out}}) = (12 \pm \sqrt{12})/3250 \quad (2)$$

where we find $\tau_{\downarrow,out}$ = 162 ± 41s. For D1, we estimate $\tau_{\downarrow,out}$ by performing an additional readout step after the electron was initialised to $|\downarrow\rangle$ from the previous readout step. Over a readout time of t_1 = 500 ms we measure 87 out of 7500 current pulses due to a $|\downarrow\rangle$ electron tunnelling out of the donor dot. Therefore the tunnel out time $\tau_{\downarrow,out}$ is found by solving

$$\exp(\frac{-t_1}{\tau_{\downarrow,out}}) = 1 - (87 \pm \sqrt{87})/7500 \quad (3)$$

where we find $\tau_{\downarrow,out}$ = 99 ±11 s.

The $|\downarrow\rangle$ tunnel out time can also be estimated from [*25*]

$$\tau_{\downarrow,out} = \tau_{\downarrow,in} \frac{p(E)}{1 - p(E)} \quad (4)$$

where $p(E) = (1 + \exp((E - E_F)/k_b T_e)^{-1}$ is the occupation probability of the SET as a function of energy *E*. In the case where the Fermi level of the SET is aligned directly between the Zeeman split electrochemical potentials, $E - E_F = \mu_{0\leftrightarrow\downarrow} - E_F = -1/2\ E_Z$, from (4) we estimate the ↓ tunnel out time to be $\tau_{\downarrow,out}$ = 20 s using the experimental vales for the electron temperature of T_e = 100 mK, the magnetic field of B = 1.5 T, and the ↓ tunnel in time of $\tau_{\downarrow,in}$ = 10 ms. If we modify the readout position to the extreme case where the Fermi energy of the SET is aligned with the ↑ electrochemical potential giving $E - E_F = \mu_{0\leftrightarrow\downarrow} - E_F = -E_Z$, then the ↓ tunnel out time increases to $\tau_{\downarrow,out}$ = 43000s. At this position it is more likely that after the ↑ electron tunnels out of the donor another ↑ electron will tunnel back in. However this does not affect the spin readout as it still results in a pulse in the SET current for only ↑ electrons. Although it may appear that this is then the best position for readout, the argument assumes that $\tau_{\downarrow,in}$ and $\tau_{\uparrow,out}$ remain constant if we change the readout position. However, $\tau_{\downarrow,in}$ will decrease reducing our estimated $\tau_{\downarrow,out}$. Furthermore, $\tau_{\uparrow,out}$ will increase leading to longer readout times and more errors during the spin to charge conversion process. In the actual experiment we operated in between these two cases.

The total readout fidelity is determined by the spin to charge conversion fidelity and the electrical fidelity. The spin to charge conversion fidelity for a $|\downarrow\rangle$ (β) electron is determined by the errors due to a $|\downarrow\rangle$ electron tunnelling out of the donor resulting in the incorrect assignment of a $|\downarrow\rangle$ with a $|\uparrow\rangle$. The spin to charge conversion fidelity for a $|\uparrow\rangle$ (α) electron is determined by the errors due to a $|\uparrow\rangle$ electron relaxing to a $|\downarrow\rangle$ or not tunnelling out of the donor resulting in the incorrect assignment of a $|\uparrow\rangle$ with

a $|\downarrow\rangle$. The fidelities β and α for the spin to charge conversion of a $|\downarrow\rangle$ or $|\uparrow\rangle$ electron, respectively, can be calculated analytically using the following expressions [*25*]

$$\beta = \exp\left(\frac{-\Delta t}{\tau_{\downarrow,\text{out}}}\right) \tag{4}$$

$$\alpha = \frac{1}{\tilde{T}^2}\left[\tilde{T}^2 - \frac{\tau_{\uparrow,\text{out}}\tau_{\downarrow,\text{out}}}{\exp\left(\frac{\Delta t}{\tau_{\downarrow,\text{out}}}\right)} - \frac{T_1\tau_{\downarrow,\text{out}}}{\exp\left(\frac{\Delta t}{\tau_{\uparrow,\text{out}}}\right)\exp\left(\frac{\Delta t}{T_1}\right)} + \frac{T_1\tau_{\uparrow,\text{out}}}{\exp\left(\frac{\Delta t}{\tau_{\uparrow,\text{out}}}\right)\exp\left(\frac{\Delta t}{T_1}\right)}\right] \tag{5}$$

where $\tilde{T}^2 = T_1\tau_{\downarrow,\text{out}} - T_1\tau_{\uparrow,\text{out}} + \tau_{\downarrow,\text{out}}\tau_{\uparrow,\text{out}}$.

Figure S5a, b shows the spin to charge conversion fidelities as a function of readout time Δt. The average fidelity (α + β)/2 (black line) is optimised for a readout time of Δt = 58 ms (62 ms) giving β = 99.95% (99.95%) and α = 99.93% (99.95%) for the readout of D1 (D2).

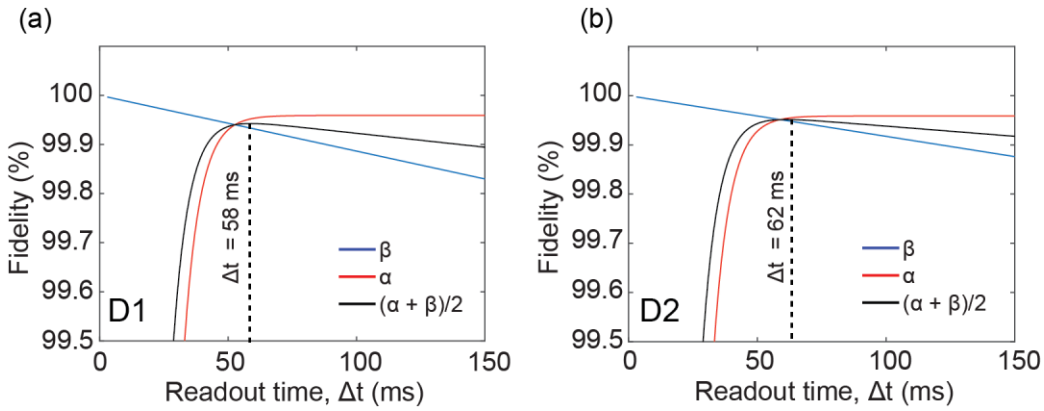

fig. S5. Optimization of the readout time. The spin to charge conversion fidelities β (blue line) and α (red line) as a function of readout time Δt for the first electron bound to (**a**) D1 and (**b**) D2. The black line shows the average fidelity and is maximum at the optimal D1 and D2 readout times of Δt = 58 ms and Δt = 62 ms, respectively.

During readout, the spin of the electron is assigned to $|\uparrow\rangle$ if the current rises above the threshold current I_t which is optimised to give the maximum measurement fidelity. The electrical fidelities $F_\uparrow$ and $F_\downarrow$ of the readout of a $|\uparrow\rangle$ and $|\downarrow\rangle$ electron are determined by the errors involved in this detection process which include $|\uparrow\rangle$ current pulses being missed due to the finite bandwidth of the measurement and electrical noise resulting in a $|\downarrow\rangle$ being accidentally detected as a $|\uparrow\rangle$. Although increasing the bandwidth will reduce $|\uparrow\rangle$ errors, it will also result in more electrical noise increasing the $|\downarrow\rangle$ errors. Consequently, a compromise is made in the measurement bandwidth (10 kHz) used in the readout measurements to minimise both the $|\uparrow\rangle$ and $|\downarrow\rangle$ electrical errors.

To calculate the electrical readout fidelity for the first electron bound to D1 we record the peak current I_{peak} during the optimised readout time of Δt = 58 ms for 7500 readout cycles. In fig. S6a, a histogram $N(I)$ of the recorded peak current (black circles) shows two well-resolved peaks which correspond to the detection of a $|\downarrow\rangle$ (lower current peak) and $|\uparrow\rangle$ (higher current peak) electron. To separate $N(I)$ into histograms of the peak current for $|\downarrow\rangle$ $N_\downarrow(I)$ and $|\uparrow\rangle$ $N_\uparrow(I)$ we perform numerical modelling where we simulate 100,000 SET current traces [*23, 25*]. The shape of these traces are constructed from the experimentally extracted tunnel rates $\tau_{\uparrow,out}$ = 5.7 ± 0.4 ms, $\tau_{\downarrow,in}$ = 11.6 ± 1.0 ms and the measured current pulse height ΔI = 153 pA. To each trace we add Gaussian noise with standard deviation A_n which is treated as a fitting parameter. This is followed by numerically filtering equivalent to the analogue low pass filtering in the experiment - an 8th order Bessel filter with a cut-off frequency of f_c = 10 kHz. Knowing the initial spin state for each of these simulated traces we can calculate $N_\downarrow(I)$ and $N_\uparrow(I)$ shown by the blue and purple line in fig. S5a. The sum of these probabilities gives $N(I) = N_\downarrow(I) + N_\uparrow(I)$ which we fit to the experimental data. For the best fit we find A_n = 0.4 pA Hz$^{-1/2}$ and the probability of initializing the spin to $|\uparrow\rangle$ to be N_0 = 0.46.

The $|\downarrow\rangle$ and $|\uparrow\rangle$ electrical fidelities $F_\downarrow$ and $F_\uparrow$ as a function of threshold current shown in fig. S6c were calculated from the simulated $N_\downarrow(I)$ and $N_\uparrow(I)$ with the following integrals $F_\downarrow = 1 - \int_{I_t}^{\infty} N_\downarrow(I)dI$ and $F_\downarrow = 1 - \int_{-\infty}^{I_t} N_\uparrow(I)dI$ [*23*]. The electrical readout visibility is defined as $V = F_\downarrow + F_\uparrow - 1$. For the threshold current that maximises the visibility, we find the electrical fidelities of D1 to be $F_\downarrow$ = 100% and $F_\uparrow$ = 99.8%. Using the same numerical model (see fig. S6b, d) we find the electrical fidelities of the readout of the first electron bound to D2 to be $F_\downarrow$ = 100% and $F_\uparrow$ = 99.7%. In the fit we use the parameters N_0 = 0.44, A_n = 0.4 pA Hz$^{-1/2}$, Δt = 62 ms, $\tau_{\uparrow,out}$ = 5.9 ± 0.4 ms and $\tau_{\downarrow,in}$ = 8.2 ± 0.8 ms. The total measurement fidelity is defined as $F_m = (\beta F_\downarrow + \alpha F_\uparrow)/2$ [*4*] giving F_m = 99.8% for D1 and F_m = 99.8% for D2, demonstrating high fidelity single-shot readout of the electron bound to each donor dots.

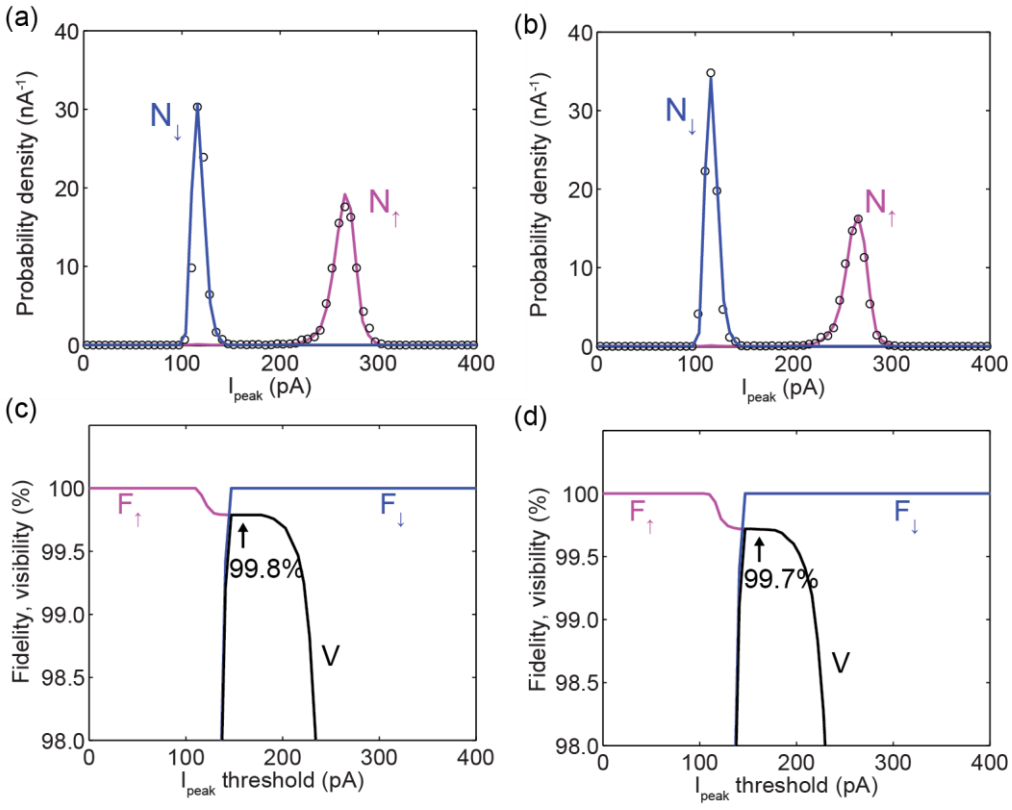

fig. S6. Electrical readout fidelity of D1 and D2. (**a**–**b**) Histograms of the current response maxima I_{peak} during the readout of the first electron bound to (a) D1 and (b) D2 for a fixed time interval of Δt = 58 ms and Δt = 62 ms. These distributions are fitted with the sum of two histograms $N_{\uparrow}$ (pink) and $N_{\downarrow}$ (blue) calculated through the numerical simulation of the data set in fig. S4. (**c**–**d**). The electrical readout fidelities and visibility of the (c) D1 and (d) D2 readout as a function of the threshold current.

section S3. Comparison of the spin relaxation times of previous donor devices

In fig. S7 we compare spin relaxation rates as a function of magnetic field for all previously published STM patterned [*2*, *25*] and Si-MOS ion implanted donor devices [*24*, *26*]. Almost all devices show a clear deviation from the B^5 field dependence at lower fields once the spin relaxation times are between 0.2 ms to 5 s (grey shaded region). Interestingly, the field dependence of Device A from [*24*] (light blue triangles in fig. S7) is very similar to the 2P and 3P (blue and red square in fig. S7) donor device presented in the main manuscript suggesting the same relaxation mechanism in these devices cause the B^5 deviation at low magnetic fields.

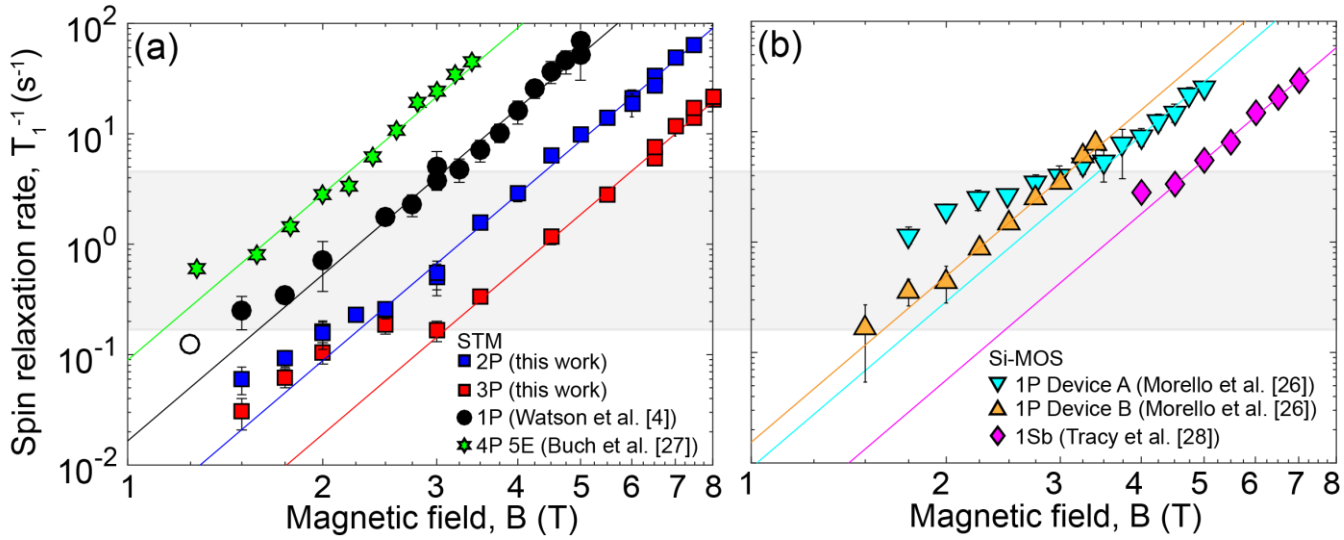

fig. S7. Deviation from the B^5 field dependence in donor devices. Spin relaxation rates of an electron spin as a function of magnetic field for previously published (**a**) STM patterned [*2*, *25*] and (**b**) Si-MOS ion implanted donor devices [*24*, *26*]. Note an additional data point (black open circle) at B = 1.25 T for the 1P device presented in [*2*] has been added from a separate cool down.